fluids

MDPI

Article

Regularized Stokeslets Lines Suitable for Slender Bodies in Viscous Flow

Boan Zhao [1,†] and Lyndon Koens [2,*,†]

[1] Department of Applied Mathematics and Theoretical Physics, University of Cambridge, Wilberforce Road, Cambridge CB3 0WA, UK; bz258@cam.ac.uk
[2] Department of Mathematics and Statistics, Macquarie University, 192 Balaclava Rd, Macquarie Park, NSW 2113, Australia
* Correspondence: lyndon.koens@mq.edu.au
† These authors contributed equally to this work.

Abstract: Slender-body approximations have been successfully used to explain many phenomena in low-Reynolds number fluid mechanics. These approximations typically use a line of singularity solutions to represent flow. These singularities can be difficult to implement numerically because they diverge at their origin. Hence, people have regularized these singularities to overcome this issue. This regularization blurs the force over a small blob and thereby removing divergent behaviour. However, it is unclear how best to regularize the singularities to minimize errors. In this paper, we investigate if a line of regularized Stokeslets can describe the flow around a slender body. This is achieved by comparing the asymptotic behaviour of the flow from the line of regularized Stokeslets with the results from slender-body theory. We find that the flow far from the body can be captured if the regularization parameter is proportional to the radius of the slender body. This is consistent with what is assumed in numerical simulations and provides a choice for the proportionality constant. However, more stringent requirements must be placed on the regularization blob to capture the near field flow outside a slender body. This inability to replicate the local behaviour indicates that many regularizations cannot satisfy the no-slip boundary conditions on the body's surface to leading order, with one of the most commonly used blobs showing an angular dependency of velocity along any cross section. This problem can be overcome with compactly supported blobs, and we construct one such example blob, which can be effectively used to simulate the flow around a slender body.

Keywords: regularized Stokeslets; Stokeslets; slender-body theory; asymptotic methods

Citation: Zhao, B.; Koens, L. Regularized Stokeslets Lines Suitable for Slender Bodies in Viscous Flow. *Fluids* **2021**, *6*, 335. https://doi.org/10.3390/fluids6090335

Academic Editors: Ricardo Cortez and Sarah D. Olson

Received: 27 August 2021
Accepted: 15 September 2021
Published: 21 September 2021

1. Introduction

Slender bodies immersed in fluids are frequently studied in biology, polymer mechanics and colloids. These bodies typically have arc length much larger than their radius and can be difficult to resolve numerically. Let a denote the ratio of the radius of a slender body to its length. In the small a limit, asymptotic theories have been developed for the flow around slender bodies [1–10]. These theories are called slender-body theories (SBTs), and they expand the system in powers of a or $1/\ln a$. Algebraically accurate SBTs have proven to be very accurate and provide exact results for prolate spheroids [3,5,7,11–16], while logarithmically accurate SBTs are useful for analytical estimations [17–24]. Many of these theories place the singularity solutions of Stokes equations along the centreline of the body. This singularity representation diverges on the centreline of the body, and it can become difficult to implement numerically.

One approach to overcome these problems is to regularize the singularities by distributing the force over a small blob [25–27]. This regularization of singularities was introduced by Cortez [25] with applications to the boundary integral representation for the flow [26,28–30]. It has since been extended to describe the flow around slender bodies by using different regularized slender-body theories [31–36].

Two major versions of these regularized SBTs exist: one in which both regularized point forces and source dipoles are distributed over the centreline [31,32,36] and one that consists of placing a series of regularized point forces along the centreline of the body [34,35,37–40]. The former uses asymptotic methods to match the boundary conditions in SBT, while the latter assumes that the regularized singularities will produce the correct flow outside the slender body with a suitable choice of regularization parameter. This is argued from unit analysis but has not been mathematically proven. Here, we investigate the accuracy of the latter representation but note that recent analysis has looked into the accuracy of the former [41].

In this paper, we compare the asymptotic flows around a line of regularized singularities to the flow around a slender body as predicted by slender-body theory. We show that the asymptotic flow far from the body can be captured by any regularization provided that the regularization parameter satisfies a specific equation that depends on the shape of the blob. This justifies the linear relationship between ϵ and the thickness of the slender body, which is typically assumed in numerical simulations. We also show that the flow close to the slender body can only be asymptotically captured for specific types of blobs. As such, not all regularization choices are capable of satisfying the no-slip boundary conditions on the body and so cannot capture the behaviour of the slender body itself. This is an issue for a commonly used power-law decaying blob but not for compactly supported blobs. We construct one such compact blob, which could be effectively used for numerical simulations.

In Section 2, we briefly review Stokes flow with a focus on classical and regularized singularity solutions and slender-body theories. Section 3 then identifies the conditions under which the asymptotic flow far from a line of regularized Stokeslets is the same as that far from a slender body before we identify the conditions necessary to capture the near flow in Section 4. Finally, we look at how these conditions apply to typical blob types in Section 5 before we conclude the paper.

2. Background into Viscous Flows around Slender Bodies

2.1. Stokes Flow and Classical Singularity Solutions

At microscopic scales the ratio of fluid inertia to fluid viscosity, the Reynolds number tends to be very small. In these cases, the behaviour of the resultant slow viscous flow can be accurately described by the incompressible Stokes equations [42–44]:

$$-\nabla p + \mu \nabla^2 \boldsymbol{u} + \boldsymbol{f} = 0, \quad (1)$$

$$\nabla \cdot \boldsymbol{u} = 0, \quad (2)$$

where p is the pressure of the fluid, $\boldsymbol{u}$ is the velocity of the fluid and $\boldsymbol{f}$ is the force per unit volume on the fluid. Throughout this paper, we will set $\mu = 1$ without any loss of generality. Although these equations are linear and time independent, they display a strong dependence on the geometry of the system considered. As a result, analytical solutions to these equations are rare except in very specific geometries [42–44]. Hence, for a typical problem, they must be evaluated numerically or asymptotically. Both of these approaches often use the point force solution to the flow.

The fluid flow from a point force, $\boldsymbol{f} = \boldsymbol{F}\delta(\boldsymbol{r})$ where $\delta(\boldsymbol{r})$ is the three dimensional Dirac delta function supported at the origin, in a viscous fluid is called the Stokeslet and, in free space, generates the following flow:

$$\boldsymbol{u}(\boldsymbol{r}) = \boldsymbol{S}(\boldsymbol{r}) \cdot \boldsymbol{F} = \left(\frac{r^2 \boldsymbol{I} + \boldsymbol{r}\boldsymbol{r}}{8\pi r^3} \right) \cdot \boldsymbol{F}, \quad (3)$$

$$p(\boldsymbol{r}) = \boldsymbol{P}(\boldsymbol{r}) \cdot \boldsymbol{F} = \left(\frac{\boldsymbol{r}}{4\pi r^3} \right) \cdot \boldsymbol{F}, \quad (4)$$

where $\boldsymbol{r}$ is the position vector, $r = |\boldsymbol{r}|$ is its norm, $\boldsymbol{S}(\boldsymbol{r})$ is the Oseen tensor, $\boldsymbol{I}$ is the identity tensor and all tensor product symbols are omitted. The Stokeslet is the Green's function of

the flow and satisfies the Stokes equations everywhere outside the origin at which point it diverges. As a result, it can be used to solve the Stokes equations in two different ways: the boundary integral representation and the representation by fundamental singularities [42,44]. In the boundary integral representation, the Green's function nature of the Stokeslet is used to convert the equations into an integral over the boundary of the domain. These integrals can then be discretized to solve for the unknowns in the problem in a method called the boundary element method (for more information on this method see Reference [44]).

The representation by fundamental singularities method, on the other hand, seeks to place the Stokeslet and its derivatives outside of the flow region (i.e., within the body) such that the boundary conditions are satisfied [45]. If such a distribution can be found, it is guaranteed to be the solution due to the uniqueness of Stokes flow. In general, the specific singularities needed depend on the geometry of the problem, the region they are distributed over and the motion of the body. However, due to the biharmonic nature of the Stokes equations, singularity representations involving the Stokeslet are consistently found to occur in combination with another singularity solution called the source dipole. The source dipole is proportional to the Laplacian of the Stokeslet and generates the following flow:

$$\boldsymbol{u}(\boldsymbol{r}) = \boldsymbol{D}(\boldsymbol{r}) \cdot \boldsymbol{A} = \frac{r^2\boldsymbol{I} - 3\boldsymbol{r}\boldsymbol{r}}{8\pi r^5} \cdot \boldsymbol{A}, \tag{5}$$

$$p(\boldsymbol{r}) = 0, \tag{6}$$

where $\boldsymbol{A}$ is the strength of the source dipole, and $\boldsymbol{D}(\boldsymbol{r}) = \nabla^2 \boldsymbol{S}(\boldsymbol{r})/2$ is the source dipole tensor. Similar to the Stokeslet, this fundamental singularity satisfies the Stokes equations everywhere except at the origin where it diverges.

2.2. Regularized Singularity Solutions

The divergent nature of the Stokeslets requires special care when integrating over or determining the flow close to the origin. However this integration is necessary for the boundary integral representation, and the nearby flow is often required when constructing representations using fundamental singularities. Cortez proposed the regularization of these singularities to overcome this issue [25]. This was achieved by replacing the Dirac delta function in the point force representation by a suitable mollifier (hereafter called a blob), $f_\epsilon(\boldsymbol{r}) = \epsilon^{-3} f(\boldsymbol{r}/\epsilon)$ where $\iiint f_\epsilon(\boldsymbol{r})\, d\boldsymbol{r} = 1$, that depends on some regularization parameter ϵ. As $\epsilon \to 0$, these blobs become the Dirac delta function; thus, the flow from a Stokeslet is recovered. The flow from a specific blob can be found by solving the forced Stokes equations or represented as a convolution with the relevant singularity. For example, the regularized Oseen tensor can be generally expressed as:

$$\boldsymbol{S}^\epsilon(\boldsymbol{r}) = \boldsymbol{S} * f_\epsilon = \int \boldsymbol{S}(\boldsymbol{r} - \boldsymbol{r}') f_\epsilon(\boldsymbol{r}') d\boldsymbol{r}' \tag{7}$$

but a popular regularization takes the following form:

$$\boldsymbol{S}^\epsilon(\boldsymbol{r}) = \frac{\boldsymbol{I}(r^2 + 2\epsilon^2) + \boldsymbol{r}\boldsymbol{r}}{8\pi r_\epsilon^3}, \qquad r_\epsilon = \sqrt{r^2 + \epsilon^2} \tag{8}$$

when the blob is $f_\epsilon(r) = 15\epsilon^4/(8\pi r_\epsilon^7)$. The flow from these tensors define the regularized Stokeslet.

The substitution of this regularized Stokeslet into the boundary integral representation develops the regularized boundary element method. This method overcomes any singularity issues caused by the Stokeslet but introduces an error related to the regularization parameter ϵ [26]. Careful analysis of this error showed that, for spherically symmetric blobs, the additional error in the boundary integral representation is proportional to ϵ^2 [30].

This error can be understood through the additional flows generated by the regularization process [27]. We previously showed that when $r \gg \epsilon$, the regularized Stokeslet S^ϵ can be written as an infinite sum of singularity solutions, and when $r \ll \epsilon$ it becomes

isotropic. Furthermore, when f is spherically symmetric, the regularized Oseen tensor can be expressed exactly [27] as:

$$\boldsymbol{S}^{\epsilon}(\boldsymbol{r}) = \boldsymbol{S}(\boldsymbol{r}) \int_0^{r/\epsilon} 4\pi t^2 f(t)dt + \epsilon^2 \boldsymbol{D}(\boldsymbol{r}) \int_0^{r/\epsilon} \frac{4\pi}{3} t^4 f(t)dt + \frac{2\boldsymbol{I}}{3\epsilon} \int_{r/\epsilon}^{\infty} t f(t)dt, \tag{9}$$

where we have now expressed it in terms of fundamental singularity solutions to the Stokes equations. The above representation shows that the flow far from a regularized Stokeslet can always be expressed as that of a Stokeslet and a source dipole proportional to ϵ^2 regardless of the choice of blob. Hence, a spherically symmetric blob generally produces additional flows at order ϵ^2.

This ϵ^2 error can be controlled by keeping ϵ much smaller than all other length scales within a given problem, thereby allowing the benefits of regularization to outweigh any drawbacks. As such, regularized boundary element simulations have become an increasingly popular tool to explore the behaviour of micro-swimmers [28,34,37–39,46,47] and have been extended beyond free space singularities [46,48,49]. This process has proved very popular and has been extended to create regularised slender-body theories [31–33,35,36,40].

2.3. Classical Slender-Body Theory

The slow viscous hydrodynamics of long thin bodies is important in many systems [2]. However, this slender-body hydrodynamics can be hard to simulate thanks to the very large aspect ratio $1/a$ (major/minor lengths) of the body. This large aspect ratio causes boundary element methods to typically require high surface resolutions. Hence, asymptotic methods, called slender-body theories (SBTs), have been developed to overcome these issues [1–7,10]. These theories seek to expand the governing equations in terms of the large aspect ratio $1/a$ to produce simplified models for the hydrodynamics. Broadly, SBTs have been divided into two types: those that expand the system in powers of $1/\ln(a)$ [1,3] and those that expand the system in powers of a [4–7]. The former is often called resistive force theory and provides useful analytical estimates [17–24], while the latter has been shown to provide highly accurate results in numerous situations [11–16].

Probably the most commonly used algebraically accurate SBT was first developed by Keller and Rubinow [4]. This version was developed by matching the flow around an infinite cylinder to that of a line of Stokeslets. These equations were later rederived and extended by Johnson [5] and Gotz [6] by using the representation of fundamental singularities and matched asymptotic expansions. They achieved this by parametrizing the surface of the slender body, $\boldsymbol{x}_S(s,\theta)$, as:

$$\boldsymbol{x}_S(s,\theta) = \boldsymbol{x_0}(s) + a\boldsymbol{e_r}(s,\theta)\rho_0(s), \tag{10}$$

where $s \in [0,1]$ is the arclength parameter of the centreline, $\boldsymbol{x_0}(s)$ is the centreline of the body, $0 \leq a\rho_0(s) \leq a$ is the body radius at s, $\boldsymbol{e_t} = \dot{\boldsymbol{x_0}}/|\dot{\boldsymbol{x_0}}|$ is the unit tangent vector along the centreline and $\boldsymbol{e_r}(s,\theta)$ is the local radial vector perpendicular to $\boldsymbol{e_t}$ (Figure 1). The radial vector, $\boldsymbol{e_r}$, is often represented through the Frenet–Serret coordinates as $\boldsymbol{e_r}(s,\theta) = \cos(\theta)\hat{\mathbf{n}} + \sin(\theta)\hat{\mathbf{b}}$, where $\hat{\mathbf{n}}$ and $\hat{\mathbf{b}}$ are the normal and bi-normal vectors relative to the centreline, respectively. Johnson and Gotz assumed that the leading-order flow around such a body could be captured by a system of Stokeslets with strength $\boldsymbol{\alpha}^S(s)$ and source dipoles with strength $\boldsymbol{\beta}^S = \frac{1}{2}a^2\rho_0^2\boldsymbol{\alpha}^S$ placed along the body's centreline, $\boldsymbol{x_0}(s)$. This choice of singularity representation comes from the exact solutions known for a prolate spheroid [45] and generates the following flow:

$$\boldsymbol{u}(\boldsymbol{x}) = \int_0^1 \boldsymbol{S}(\boldsymbol{x} - \boldsymbol{x_0}(t)) \cdot \boldsymbol{\alpha}^S(t) + \boldsymbol{D}(\boldsymbol{x} - \boldsymbol{x_0}(t)) \cdot \boldsymbol{\beta}^S(t)dt. \tag{11}$$

The uniqueness of Stokes flow tells us that this representation must be the solution if the fluid velocity $\boldsymbol{u}(\boldsymbol{x})$ matches the surface velocity of the body when $\boldsymbol{x} = \boldsymbol{x_S}$. They then

assumed that the surface velocity, $\boldsymbol{U}(s)$, is uniform along each cross-section (i.e., it only depends on the position along the centreline $\boldsymbol{x_0}$) and performed a matched asymptotic expansion for $\boldsymbol{u}(\boldsymbol{x_S})$ in the limit $a \to 0$ while keeping s, and θ fixed.

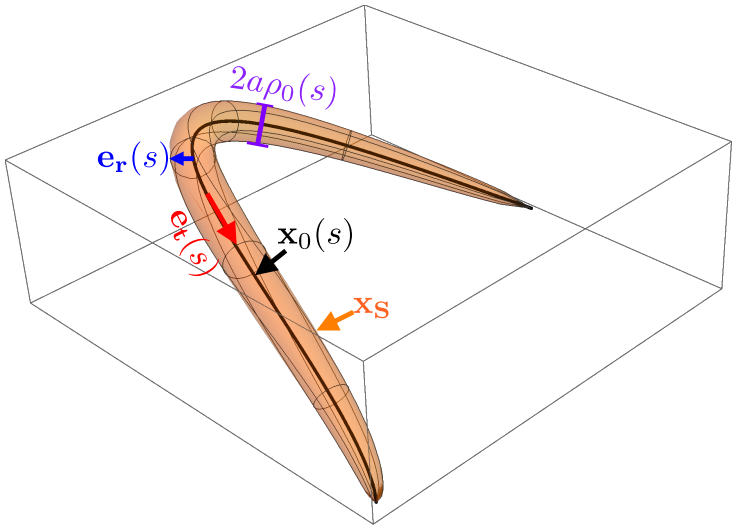

Figure 1. Example geometry of a slender body. $\boldsymbol{x}_0(s)$ is the centreline, $\boldsymbol{x_S}$ is the surface, $\boldsymbol{e_t}(s)$ is the tangent to the centreline, $\boldsymbol{e_r}(s)$ is a radial vector perpendicular to the tangent and $2a\rho_0(s)$ represents the thickness at s.

This matched asymptotic expansion divided the system into an outer and an inner region, and it expanded the behaviour in each region in the limit $a \to 0$. The different regions are then matched together by using Van Dyke's matching rule, and a composite representation formed [50]. We will provide a summary of the major results of this expansion here and refer readers to the thesis of Gotz [6] for the full derivation. In the inner region, $\xi = (t-s)/a$ is held constant, and the integral kernels expand to:

$$\boldsymbol{S}^{(i)}(\boldsymbol{x_S} - \boldsymbol{x_0}(t)) = \frac{\boldsymbol{I}}{8\pi a\delta_0} + \frac{\rho_0^2 \boldsymbol{e_r e_r} - \rho_0\xi(\boldsymbol{e_r e_t} + \boldsymbol{e_t e_r}) + \xi^2 \boldsymbol{e_t e_t}}{8\pi a\delta_0^3} + O(1), \tag{12}$$

$$\boldsymbol{D}^{(i)}(\boldsymbol{x_S} - \boldsymbol{x_0}(t)) = \frac{\boldsymbol{I}}{8\pi a^3\delta_0^3} - 3\frac{\rho_0^2 \boldsymbol{e_r e_r} - \rho_0\xi(\boldsymbol{e_r e_t} + \boldsymbol{e_t e_r}) + \xi^2 \boldsymbol{e_t e_t}}{8\pi a^3\delta_0^5} + O(a^{-2}), \tag{13}$$

$$\boldsymbol{\alpha}^S(t) = \boldsymbol{\alpha}^S(s) + O(a), \tag{14}$$

where the superscript (i) denotes the inner region expanded form and $\delta_0(t,s,a) = \sqrt{\xi^2 + \rho_0^2(s)}$. Similarly, the outer limit fixes t and produces the expanded forms:

$$\boldsymbol{S}^{(o)}(\boldsymbol{x_S} - \boldsymbol{x_0}(t)) \cdot \boldsymbol{\alpha}^S(t) = \frac{1}{8\pi}\frac{\boldsymbol{\alpha}^S(t)}{R_0} + \frac{1}{8\pi}\frac{\boldsymbol{R_0 R_0 \alpha}^S(t)}{R_0^3} + O(a), \tag{15}$$

$$\boldsymbol{D}^{(o)}(\boldsymbol{x_S} - \boldsymbol{x_0}(t)) \cdot \boldsymbol{\beta}^S(t) = \boldsymbol{0} + O(a), \tag{16}$$

where the superscript (o) denotes the outer region expanded term, $\boldsymbol{R_0}(t,s) = \boldsymbol{x_0}(s) - \boldsymbol{x_0}(t)$, and its norm is $R_0 = |\boldsymbol{R_0}|$. The common part of these two asymptotic forms is found by expanding the outer form in terms of the inner regions variables or equivalently the inner form in terms of the outer regions variables [50], and it is given by:

$$\boldsymbol{S}^{(o)\in(i)}(\boldsymbol{x_S} - \boldsymbol{x_0}(t)) \cdot \boldsymbol{\alpha}^S(t) = \boldsymbol{S}^{(i)\in(o)}(\boldsymbol{x_S} - \boldsymbol{x_0}(t)) \cdot \boldsymbol{\alpha}^S(t) = \frac{\boldsymbol{\alpha}^S(s)}{8\pi|s-t|} + \frac{\boldsymbol{e_t e_t} \cdot \boldsymbol{\alpha}^S(s)}{8\pi|s-t|} + O(a), \tag{17}$$

$$\boldsymbol{D}^{(o)\in(i)}(\boldsymbol{x_S} - \boldsymbol{x_0}(t)) \cdot \boldsymbol{\beta}^S(t) = \boldsymbol{D}^{(i)\in(o)}(\boldsymbol{x_S} - \boldsymbol{x_0}(t)) \cdot \boldsymbol{\beta}^S(t) = \boldsymbol{0} + O(a), \tag{18}$$

where the superscript $(o) \in (i)$ denotes the outer asymptotic representations, Equations (15) and (16), expanded in the inner region variables ξ, and $(i) \in (o)$ denotes the inner asymptotic representations, Equations (12) and (13), expanded in the outer region variable t.

Since these regions match a composite representation, the integral can be formed by adding the inner and outer limits, subtracting the common part and then integrating the representation over the entire length. By integrating this composite representation, we find that the flow on the surface of the body is asymptotically given by:

$$\begin{aligned}
\boldsymbol{u}(\boldsymbol{x}_S) = \boldsymbol{U}(s) &= \int_0^1 \left[\boldsymbol{S}(\boldsymbol{x}_S - \boldsymbol{x}_0(t)) \cdot \boldsymbol{\alpha}^S(t) + \boldsymbol{D}(\boldsymbol{x}_S - \boldsymbol{x}_0(t)) \cdot \boldsymbol{\beta}^S(t) \right] dt \\
&= \int_0^1 \left[\boldsymbol{S}^{(o)}(\boldsymbol{x}_S - \boldsymbol{x}_0(t)) \cdot \boldsymbol{\alpha}^S(t) + \boldsymbol{D}^{(o)}(\boldsymbol{x}_S - \boldsymbol{x}_0(t)) \cdot \boldsymbol{\beta}^S(t) \right] dt \\
&\quad + \int_0^1 \left[\boldsymbol{S}^{(i)}(\boldsymbol{x}_S - \boldsymbol{x}_0(t)) \cdot \boldsymbol{\alpha}^S(s) + \boldsymbol{D}^{(i)}(\boldsymbol{x}_S - \boldsymbol{x}_0(t)) \cdot \boldsymbol{\beta}^S(s) \right] dt \\
&\quad - \int_0^1 \left[\boldsymbol{S}^{(o)\in(i)}(\boldsymbol{x}_S - \boldsymbol{x}_0(t)) \cdot \boldsymbol{\alpha}^S(s) + \boldsymbol{D}^{(o)\in(i)}(\boldsymbol{x}_S - \boldsymbol{x}_0(t)) \cdot \boldsymbol{\beta}^S(s) \right] dt \\
&\quad + O(a) \\
&= \frac{1}{8\pi} \int_0^1 \left[\frac{\boldsymbol{\alpha}^S(t)}{R_0} + \frac{\boldsymbol{R_0 R_0} \cdot \boldsymbol{\alpha}^S(t)}{R_0^3} - \frac{\mathbf{I} + \boldsymbol{e_t e_t}}{|s-t|} \cdot \boldsymbol{\alpha}^S(s) \right] dt \\
&\quad + \int_0^1 \left[\boldsymbol{S}^{(i)}(\boldsymbol{x}_S - \boldsymbol{x}_0(t)) \cdot \boldsymbol{\alpha}^S(s) + \boldsymbol{D}^{(i)}(\boldsymbol{x}_S - \boldsymbol{x}_0(t)) \cdot \boldsymbol{\beta}^S(s) \right] dt \\
&\quad + O(a),
\end{aligned} \tag{19}$$

where we have explicitly substituted the forms of the outer and common parts of the expansion. The remaining integrals over the inner region expansion can be asymptotically evaluated [6,7] in order to find the following:

$$\begin{aligned}
8\pi \boldsymbol{U}(s) &= \int_0^1 \left[\frac{\boldsymbol{\alpha}^S(t)}{R_0} + \frac{\boldsymbol{R_0 R_0} \cdot \boldsymbol{\alpha}^S(t)}{R_0^3} - \frac{\mathbf{I} + \boldsymbol{e_t e_t}}{|s-t|} \cdot \boldsymbol{\alpha}^S(s) \right] dt \\
&\quad + [L(\boldsymbol{I} + \boldsymbol{e_t e_t}) + (\boldsymbol{I} - 3\boldsymbol{e_t e_t})] \cdot \boldsymbol{\alpha}^S(s) + O(a),
\end{aligned} \tag{20}$$

where $L = \ln[4s(1-s)/a^2\rho_0^2]$. The above equation is the classical slender-body theory integral equation for the unknown Stokeslet strengths $\boldsymbol{\alpha}^S(t)$. These equations have been used successfully in the modeling of several systems [12–16,51–53], and have been rederived from the boundary integral representation [7] and extended to treat bodies of different shapes [54,55]. Recent studies have also studied the effectiveness of these equation in different situations and bounded error on the flow from a given force to $O(a \ln a)$ [56–58].

Once the force per unit length along the slender body is found from Equation (20), the resultant flow can be determined with Equation (11). This predicted flow has been shown to compare well with experiments of rotating helices [11] and should generally be accurate in regions close to the slender body or far away from the slender body. This is because it must asymptotically satisfy the no-slip boundary condition on the surface of the body, and the flow can be represented by a multipole expansion with Stokeslets and source dipoles far away.

Although the classic SBT equations, Equations (11) and (20), have been very successful, the components of the integrand within Equation (20) are individually divergent. Held together, these divergent factors asymptotically cancel, but this makes them difficult to treat numerically. Furthermore, the operator is known to encounter numerical instabilities related to eigenvalues changing sign. Hence, people have created regularized slender-body theories to overcome these issues.

2.4. Regularized Slender-Body Theories

The numerical issues in implementing the classical SBT equations have prompted people to create classical SBT like models using regularized Stokeslets. Two methods have been developed for this process: one where the flow is represented by a line of regularized Stokeslets and regularized source dipoles [31,32,36] and one where the flow is represented by a line of regularized Stokeslets alone [35]. Although both are based on regularized singularities, these methods treat the no-slip boundary condition and the regularization parameter very differently.

The former method, with regularized Stokeslets and regularized source dipoles, seeks to choose the source dipole strength such that the no-slip boundary condition asymptotically applies at the surface of the body. This can be shown with a similar asymptotic expansion, as is performed in the classical case. These methods can leave the regularization parameter free [32] or use it to help with the expansion [31]. In both cases, however, the regularization parameter, ϵ, helps remove the numerical issue with the implementation. The flow predicted by this method, therefore, satisfies the boundary conditions at the surface of the body and far from it but has been shown to exhibit an additional $O(1)$ difference between it and the classical SBT that cannot be fixed with the choice of regularization parameter [41]. In practice, this difference may be small and likely stems from the fact that the flow outside the body is not described by the unforced incompressible Stokes equations.

The latter method, with a line of regularized Stokeslets alone, tries to use the regularization parameter itself to capture the thickness of the slender body [35]. As such, the regularization parameter is typically chosen to be $\epsilon = ka\rho_0(s)$, where k is some arbitrary constant. The strength of the Stokeslets is then set by applying the velocity condition on an effective line in space. Often this line is chosen to be the centreline of the body, although it could be applied on a line along the surface as well. This writes the problem as a line integral similar to that of classical SBT. Similarly to the previous representation, the use of regularized Stokeslets means that the flow predicted by this model will not satisfy the unforced incompressible Stokes equations outside the body for all regularizations. However, the difference between the classical SBT prediction and that from this representation has not been determined.

In the remaining sections of this paper, we will investigate how well a line distribution of regularized Stokeslets replicates the flow around a slender body for a general spherically symmetric blob and regularization parameter. This will provide us with a set of conditions that must be met in order for the far and near field flows to asymptotically reflect that around a slender body. Importantly we show that one common power-law blob cannot satisfy the no-slip condition on the body's surface, while compactly supported blobs do.

3. Regularizations for the Flow Far from a Slender Body

Far away from the slender body, the flow, predicted by SBT, is well approximated by Equation (11). This is the because it is a leading order multipole representation [11]. Similarly, the flow far from a line of regularized Stokeslets placed along the centreline of the body can be approximated by expanding $\boldsymbol{S}^{\epsilon}(\boldsymbol{x}-\boldsymbol{x_0}(t))$ in the limit $|\boldsymbol{x}| \gg 1, \epsilon$ and integrating over the length. This expansion provides the following:

$$\begin{aligned}\boldsymbol{u}_{\epsilon\text{far}}(\mathbf{x}) &= \int_0^1 \boldsymbol{S}(\boldsymbol{x}-\boldsymbol{x_0}(t))\cdot\boldsymbol{\gamma}(t)\,dt + O\left(\frac{1}{|\boldsymbol{x}|^2}\right) \\ &\quad + \left[\epsilon^2\left(\int_0^\infty \frac{4\pi}{3}u^4 f(u)\,du\right)\right]\int_0^1 \boldsymbol{D}(\boldsymbol{x}-\boldsymbol{x_0}(t))\cdot\boldsymbol{\gamma}(t)\,dt + O\left(\frac{\epsilon^2}{|\boldsymbol{x}|^4}\right), \quad (21)\end{aligned}$$

where $\boldsymbol{u}_{\epsilon\text{far}}(\mathbf{x})$ is the far field flow from the line of regularized Stokeslets, and we have used Equation (9). The above approximation assumes that the functions are well behaved enough to interchange limits and integrals. We note that the source dipole term is subdominate to the Stokeslet in the far-field limit. However, we retain both contributions here because

the Stokeslet and source dipole generate different flows, and the far-field contributions of both singularities, from the motion of a slender body, are asymptotically determined by Equation (11). If we compare the Stokeslet and source dipole flows, we observe that the above equation approximates Equation (11) if the following holds:

$$\gamma(t) = \boldsymbol{\alpha}(t), \tag{22}$$

$$2h(s)^2\left(\int_0^\infty \frac{4\pi}{3}u^4 f(u)du\right) = \rho_0(s)^2, \tag{23}$$

where we have set $\epsilon = ah(s) + O(a^2)$. The first condition tells us that, in order for the flow around a line of regularized Stokeslets to replicate that of a slender body, the strength of the regularized Stokeslets must be equal to the force per unit length along the body. This is unsurprising. The second equation, however, provides a relationship between the regularization parameter, $\epsilon = ah(s)$, the blob used for the regularization, $f(v)$, and the cross section of the body, $\rho_0(s)$. It shows that, as assumed in the existing literature, the regularization parameter is proportional to the radius of the cross-section and this proportionality constant depends on the fourth moment of the regularizing blob. Provided this moment exists, the far field contributions from any regularized Stokeslet can be made to approximate the Stokeslet and source dipole flow contributions far from a slender body.

4. Regularization's for the Flow Near a Slender Body

The flow from a line of regularized Stokeslets near the boundary of the slender body can be approximated by using a similar matched asymptotic expansion as that in slender-body theory. This involves expanding the regularised Stokeslet kernel in the limit of small a for an inner region, where $\xi = (t-s)/a$, s and θ are fixed, and outer region, where t is fixed, and then matching the solutions. The composite representation of the integral is then found by adding the outer and inner regions and subtracting the common part, similarly to before, to find the following:

$$\begin{aligned}\int_0^1 \boldsymbol{S}^\epsilon(\boldsymbol{x}-\boldsymbol{x_0}(t))\cdot\boldsymbol{\alpha}(t)dt &= \int_0^1 \boldsymbol{S}^{\epsilon(o)}(\boldsymbol{x}-\boldsymbol{x_0}(t))\cdot\boldsymbol{\alpha}(t)dt \\ &\quad+\int_0^1 \boldsymbol{S}^{\epsilon(i)}(\boldsymbol{x}-\boldsymbol{x_0}(t))\cdot\boldsymbol{\alpha}(s)dt \\ &\quad-\int_0^1 \boldsymbol{S}^{\epsilon(o)\in(i)}(\boldsymbol{x}-\boldsymbol{x_0}(t))\cdot\boldsymbol{\alpha}(s)dt + O(a),\end{aligned} \tag{24}$$

where the superscripts (o), (i) and $(o)\in(i)$ again denote the expansion in the outer, inner and the outer subsequently expanded in the inner (common), respectively. In the above, $\boldsymbol{x} = \boldsymbol{x_0}(s) + \boldsymbol{e_r}a\rho$ is a point close to the surface of the body, and ρ is a radial distance from the centreline that is of the same order as $\rho_0(s)$. Setting $\rho = \rho_0(s)$ corresponds to the flow on the boundary, while $\rho > \rho_0(s)$ represents the flow close to the boundary.

In the previous section, we established that far from the line of regularised Stokeslets, the kernel, $\boldsymbol{S}^\epsilon$, behaves as a line distribution of point forces and source dipoles (refer to Equation (9)). As a consequence, the outer region expansion of the regularised kernel is asymptotically equivalent to that of a Stokeslet and a source dipole in the same limits. Hence, the kernel can be expressed as:

$$\begin{aligned}\boldsymbol{S}^{\epsilon(o)}(\boldsymbol{x}-\boldsymbol{x_0}(t))\cdot\boldsymbol{\alpha}(t) &= \boldsymbol{S}^{(o)}(\boldsymbol{x}-\boldsymbol{x_0}(t))\cdot\boldsymbol{\alpha}(t) \\ &\quad+\left[\epsilon^2\left(\int_0^\infty \frac{4\pi}{3}u^4 f(u)\,du\right)\right]\boldsymbol{D}^{(o)}(\boldsymbol{x}-\boldsymbol{x_0}(t))\cdot\boldsymbol{\alpha}(t) \\ &\quad+O(a) \\ &= \frac{1}{8\pi}\frac{\boldsymbol{\alpha}^S(t)}{R_0}+\frac{1}{8\pi}\frac{\boldsymbol{R_0}\boldsymbol{R_0}\cdot\boldsymbol{\alpha}^S(t)}{R_0^3}+O(a),\end{aligned} \tag{25}$$

which is identical to the outer expanded kernel in classical SBT. In the above, we have assumed that ϵ is linearly related to a, as suggested by the analysis of the previous section. Since this outer kernel is the same as that found in classical SBT, the expansion of it in terms of the inner region variables will also be the same. The common behaviour can, therefore, be expressed as:

$$\begin{aligned} \boldsymbol{S}^{\epsilon(o)\in(i)}(\boldsymbol{x}-\boldsymbol{x_0}(t))\cdot\boldsymbol{\alpha}^S(s) &= \boldsymbol{S}^{(o)\in(i)}(\boldsymbol{x}-\boldsymbol{x_0}(t))\cdot\boldsymbol{\alpha}^S(s)+O(a) \\ &= \frac{\boldsymbol{\alpha}^S(s)}{8\pi|s-t|}+\frac{\boldsymbol{e_te_t}\cdot\boldsymbol{\alpha}^S(s)}{8\pi|s-t|}+O(a). \end{aligned} \tag{26}$$

These results can be substituted back into our composite representation for the flow near the surface of the body to find the following:

$$\begin{aligned} \int_0^1 \boldsymbol{S}^{\epsilon}(\boldsymbol{x}-\boldsymbol{x_0}(t))\cdot\boldsymbol{\alpha}(t)dt &= \frac{1}{8\pi}\int_0^1\left[\frac{\boldsymbol{\alpha}(t)}{R_0}+\frac{\boldsymbol{R_0R_0}\cdot\boldsymbol{\alpha}(t)}{R_0^3}-\frac{\mathbf{I}+\boldsymbol{e_te_t}}{|s-t|}\cdot\boldsymbol{\alpha}(s)\right]dt \\ &\quad+\int_0^1 \boldsymbol{S}^{\epsilon(i)}(\boldsymbol{x}-\boldsymbol{x_0}(t))\cdot\boldsymbol{\alpha}(s)dt+O(a). \end{aligned} \tag{27}$$

The remaining inner region expansion can be deduced from Equation (9), and it takes the following form:

$$\begin{aligned} \boldsymbol{S}^{\epsilon(i)}(\boldsymbol{x}-\boldsymbol{x_0}(t)) &= \boldsymbol{S}^{(i)}(\boldsymbol{x}-\boldsymbol{x_0}(t))\int_0^{\delta/h(s)}4\pi r^2 f(r)dr \\ &\quad+a^2h^2(s)\boldsymbol{D}^{(i)}(\boldsymbol{x}-\boldsymbol{x_0}(t))\int_0^{\delta/h(s)}\frac{4\pi}{3}r^4 f(r)dr \\ &\quad+\frac{2\boldsymbol{I}}{3ah(s)}\int_{\delta/h(s)}^{\infty} rf(r)dr+O(a), \end{aligned} \tag{28}$$

where $\epsilon = ah(s)$, $\delta(t,s,a)=\sqrt{\xi^2+\rho^2(s)}$, and we noted that $r/\epsilon = a\delta(t,s,a)/\epsilon+O(a) = O(1)$. If we consider a point on the surface $\delta=\delta_0$. The above relation expresses the inner region representation of the regularized Stokeslet in terms of the inner region representation of the Stokeslet and source dipole. Similar inner region expansions were stated in the summary of SBT for flow on the surface of the body, Equations (12) and (13). The expanded form of the Stokeslet and source dipole near the surface are structurally equivalent to these but with δ_0, ρ_0 replaced with δ, ρ. Explicitly, this provides the following:

$$\boldsymbol{S}^{(i)}(\boldsymbol{x}-\boldsymbol{x_0}(t)) = \frac{\boldsymbol{I}}{8\pi a\delta}+\frac{\rho^2\boldsymbol{e_re_r}-\rho\xi(\boldsymbol{e_re_t}+\boldsymbol{e_te_r})+\xi^2\boldsymbol{e_te_t}}{8\pi a\delta^3}, \tag{29}$$

$$\boldsymbol{D}^{(i)}(\boldsymbol{x}-\boldsymbol{x_0}(t)) = \frac{\boldsymbol{I}}{8\pi a^3\delta^3}-3\frac{\rho^2\boldsymbol{e_re_r}-\rho\xi(\boldsymbol{e_re_t}+\boldsymbol{e_te_r})+\xi^2\boldsymbol{e_te_t}}{8\pi a^3\delta^5}. \tag{30}$$

These equations can be combined with Equations (28) and (27) to asymptotically determine the flow close to the surface of the slender body from a line of regularised Stokeslets.

The difference in the near body flow from a line of regularized Stokeslets and the flow around a slender body asymptotically predicted by SBT can be determined by subtracting Equation (27) from Equation (19). Since the outer and common limits are the same in each case, the difference between the leading order contributions at $\boldsymbol{x}=\boldsymbol{x}_0(s)+a\boldsymbol{e}_r(s)\rho(s)$ is:

$$\begin{aligned}
\int_0^1 \Delta\mathrm{SBT}_\epsilon\, dt &= \int_0^1 \left[\boldsymbol{S}^{(i)}(\boldsymbol{x}-\boldsymbol{x_0}(t)) + \frac{1}{2}a^2\rho_0^2(t)\boldsymbol{D}^{(i)}(\boldsymbol{x}-\boldsymbol{x_0}(t)) - \boldsymbol{S}^{\epsilon(i)}(\boldsymbol{x}-\boldsymbol{x_0}(t))\right] dt\cdot\boldsymbol{\alpha}(s) \\
&= \int_0^1 \boldsymbol{S}^{(i)}(\boldsymbol{x}-\boldsymbol{x_0}(t))\left[1-\int_0^{\delta/h(s)} 4\pi r^2 f(r)dr\right] dt\cdot\boldsymbol{\alpha}(s) \\
&\quad +\frac{1}{2}a^2\rho_0^2(s)\int_0^1 \boldsymbol{D}^{(i)}(\boldsymbol{x}-\boldsymbol{x_0}(t))\left[1-2\frac{h^2}{\rho_0^2}\int_0^{\delta/h(s)}\frac{4\pi}{3}r^4 f(r)dr\right] dt\cdot\boldsymbol{\alpha}(s) \\
&\quad -\int_0^1 \frac{2\boldsymbol{I}}{3ah(s)}\left[\int_{\delta/h(s)}^\infty rf(r)dr\right] dt\cdot\boldsymbol{\alpha}(s) \\
&= \int_0^1 \boldsymbol{S}^{(i)}(\boldsymbol{x}-\boldsymbol{x_0}(t))\left[\int_{\delta/h(s)}^\infty 4\pi r^2 f(r)dr\right] dt\cdot\boldsymbol{\alpha}(s) - \frac{2\boldsymbol{I}}{3ah(s)}\int_0^1\left[\int_{\delta/h(s)}^\infty rf(r)dr\right] dt\cdot\boldsymbol{\alpha}(s) \\
&\quad +a^2h^2(s)\int_0^1 \boldsymbol{D}^{(i)}(\boldsymbol{x}-\boldsymbol{x_0}(t))\left[\int_{\delta/h(s)}^\infty \frac{4\pi}{3}r^4 f(r)dr\right] dt\cdot\boldsymbol{\alpha}(s) \\
&\quad +a^2\left[\frac{1}{2}\rho_0^2(s) - h^2\int_0^\infty \frac{4\pi}{3}r^4 f(r)dr\right]\int_0^1 \boldsymbol{D}^{(i)}(\boldsymbol{x}-\boldsymbol{x_0}(t))\, dt\cdot\boldsymbol{\alpha}(s)
\end{aligned} \tag{31}$$

where $\int_0^1 \Delta\mathrm{SBT}_\epsilon\, dt$ is the difference between the leading order contributions relative to the near field flows from a line of regularized Stokeslets and classical SBT. This difference needs to be O(a) for the flow around a line of regularized Stokeslets to asymptotically replicate the flow predicted by SBT to the same order. Since $\boldsymbol{\alpha}(s)$ is typically unknown, this condition must hold for arbitrary $\boldsymbol{\alpha}$(s). The integrand of the above integral can be expressed as:

$$-\Delta\mathrm{SBT}_\epsilon = E_1\boldsymbol{I} + E_2\boldsymbol{e_r}\boldsymbol{e_r} + E_3\boldsymbol{e_t}\boldsymbol{e_t} + E_4(\boldsymbol{e_r}\boldsymbol{e_t} + \boldsymbol{e_t}\boldsymbol{e_r}), \tag{32}$$

where

$$E_1 = \frac{\delta^2}{ah^3}\int_1^\infty\left(\frac{2}{3}\varrho - \frac{1}{2}\varrho^2 - \frac{1}{6}\varrho^4\right)f\left(\frac{\varrho\delta}{h}\right)d\varrho + \frac{1}{8\pi a\delta^3}\left[h(s)^2\left(\int_0^\infty \frac{4\pi}{3}u^4 f(u)du\right) - \frac{1}{2}\rho_0(s)^2\right], \tag{33}$$

$$E_2 = \frac{\rho^2}{2ah^3}\int_1^\infty(\varrho^4-\varrho^2)f\left(\frac{\varrho\delta}{h}\right)d\varrho - \frac{3\rho^2}{8\pi a\delta^5}\left[h(s)^2\left(\int_0^\infty \frac{4\pi}{3}u^4 f(u)du\right) - \frac{1}{2}\rho_0(s)^2\right], \tag{34}$$

$$E_3 = \frac{\xi^2}{2ah^3}\int_1^\infty(\varrho^4-\varrho^2)f\left(\frac{\varrho\delta}{h}\right)d\varrho - \frac{3\xi^2}{8\pi a\delta^5}\left[h(s)^2\left(\int_0^\infty \frac{4\pi}{3}u^4 f(u)du\right) - \frac{1}{2}\rho_0(s)^2\right], \tag{35}$$

$$E_4 = \frac{\rho\xi}{2ah^3}\int_1^\infty(\varrho^2-\varrho^4)f\left(\frac{\varrho\delta}{h}\right)d\varrho + \frac{3\rho\xi}{8\pi a\delta^5}\left[h(s)^2\left(\int_0^\infty \frac{4\pi}{3}u^4 f(u)du\right) - \frac{1}{2}\rho_0(s)^2\right]. \tag{36}$$

In the above we used the integral substitution $r = \varrho h(s)/\delta$ to change the lower bounds of the first integrals to one and Equations (29) and (30). These E_i values represent the relative error between the flow predicted by SBT and that from the line of regularized Stokeslets in each direction. We require all four terms to integrate to $O(a)$ for the flow to match. The integral of E_4 can be shown to be $O(a)$ by parity arguments. This is because E_4 is odd in ξ, and in the asymptotic limit $a \to 0$ the integral bounds become $\pm\infty$. However, the other three terms provide non-trivial conditions on $f(u)$.

If we assume that Equation (23) is satisfied, then the conditions $\int E_{1,2,3}\,dt = O(a)$ simplify to:

$$\frac{3h^3}{2\rho^3}\int_0^1\left[E_1+\frac{1}{3}(E_2+E_3)\right]dt = \int_{-s/(a\rho)}^{(1-s)/(a\rho)}(\zeta^2+1)\left[\int_1^\infty\left(\varrho-\varrho^2\right)f\left(\frac{\varrho\rho\sqrt{1+\zeta^2}}{h}\right)d\varrho\right]d\zeta = O(a), \tag{37}$$

$$\frac{2h^3}{\rho^3}\int_0^1 E_2\,dt = \int_{-s/(a\rho)}^{(1-s)/(a\rho)}\left[\int_1^\infty(\varrho^4-\varrho^2)f\left(\frac{\varrho\rho\sqrt{1+\zeta^2}}{h}\right)d\varrho\right]d\zeta = O(a), \tag{38}$$

$$\frac{2h^3}{\rho^3}\int_0^1 E_3\,dt = \int_{-s/(a\rho)}^{(1-s)/(a\rho)}\zeta^2\left[\int_1^\infty(\varrho^4-\varrho^2)f\left(\frac{\varrho\rho\sqrt{1+\zeta^2}}{h}\right)d\varrho\right]d\zeta = O(a), \tag{39}$$

where $\zeta = \xi/\rho = (t-s)/(a\rho)$, and the equality needs to hold for $\rho \gtrsim \rho_0$. The above conditions provide a set of restrictions on the types of blobs, $f(v)$, that can replicate the near field flow around a slender body. These conditions are necessary and sufficient for the line regularized Stokeslets to agree with classical SBT to O(a) near the boundary as the integrals of E_i represent the difference between the two representations. These conditions, therefore, specify the types of regularizations that can be used in numerical simulations to asymptotically capture the flow near a slender boy. These conditions can be viewed as an integral transform into ρ, which depends on the tails of the blobs. Although the range over which these equations apply can change from blob to blob, these equations must be true when $\rho = \rho_0$. If this condition is not satisfied, the no-slip boundary condition on the surface of the body cannot be satisfied. In these cases the solutions found with the line of regularized Stokeslets cannot be assumed to relate to the real solution a priori.

5. Testing the Conditions on Common Blob Types

In the previous sections, we identified one condition on the regularization parameter, Equation (23), required to approximately match the far field flow and three conditions on the blob type, Equations (37)–(39), in order to asymptotically match the flow near the surface of the body. These conditions apply in limit that the body is long and slender and were found by comparing the asymptotic behaviour around a line of regularised Stokeslets to that predicted by SBT. Furthermore, although these latter conditions can hold for a range of ρ, we know they must hold when $\rho = \rho_0$ if the resultant flow is to approximate that of a slender body. In this section, we apply these conditions to three common regularization blob types: power-law blobs, compact blobs and exponential blobs. In each case, we identify if a line of them can be used to represent the flow from a slender body.

5.1. Power-Law Blobs

Probably the most common blob type used within the literature is the power-law type blob. These blobs are given by:

$$f_p(v) = \frac{\Gamma(n/2)}{\pi^{3/2}\Gamma((n-3)/2)}\frac{1}{(v^2+1)^{n/2}}, \tag{40}$$

where n is a integer greater then five, and $\Gamma(x)$ is the gamma function. We remind the reader that the above blob relates to the regularizing function through $f_\epsilon = \epsilon^{-3}f(\mathbf{r}/\epsilon)$. The above representation reduces to one of the most popular examples, Equation (8), when $n = 7$.

By inserting this blob into the far field flow condition, Equation (23), we find the following:

$$h(s) = \rho_0(s)\sqrt{\frac{n-5}{2}}. \tag{41}$$

This, therefore, sets the regularization the blobs must use to satisfy the far field condition. Significantly, we observe that when $n = 7$, $h(s) = \rho_0(s)$. This indicates that

the regularisation parameter ϵ should be taken as half the thickness of the slender body, as is typically assumed in numerical simulations. Similarly, the near field conditions, Equations (37)–(39), asymptotically evaluate to the following:

$$\begin{aligned}\int_{-s/(a\rho)}^{(1-s)/(a\rho)}(\zeta^2+1)\left[\int_1^\infty\left(\varrho-\varrho^2\right)f_p\left(\frac{\varrho\rho\sqrt{1+\zeta^2}}{h}\right)d\varrho\right]d\zeta &= -\frac{(n-5)^n(n-2)\left((n-5)^2+4\rho'^2\right)^{\frac{3-n}{2}}}{16\pi(n-3)\rho'^3}\\ &\quad -\frac{(n-5)^n((n-10)n-25)F_2(\rho')}{2^{n+3}\rho'^{n+2}\pi(n-1)}\\ &\quad +\frac{(n-5)^nF_1(\rho')}{2^n\rho'^n\pi}+\frac{(n-5)^{n+2}F_3(\rho')}{2^{n+2}\rho'^{n+2}\pi n}\\ &\quad +O(a), \qquad (42)\end{aligned}$$

$$\int_{-s/(a\rho)}^{(1-s)/(a\rho)}\left[\int_1^\infty(\varrho^4-\varrho^2)f_p\left(\frac{r\rho\sqrt{1+\zeta^2}}{h}\right)d\varrho\right]d\zeta = \frac{(n-5)^{n-1}\left((n-5)^2+4\rho'^2\right)^{\frac{5-n}{2}}}{32\pi\rho'^5}+O(a), \qquad (43)$$

$$\begin{aligned}\int_{-s/(a\rho)}^{(1-s)/(a\rho)}\zeta^2\left[\int_1^\infty(\varrho^4-\varrho^2)f_p\left(\frac{\varrho\rho\sqrt{1+\zeta^2}}{h}\right)d\varrho\right]d\zeta &= \frac{(n-5)^{n-1}\left((n-5)^2+4\rho'^2\right)^{\frac{5-n}{2}}}{64\pi\rho'^5}\\ &\quad -\frac{(n-5)^nF_4(\rho')}{2^{n+1}\rho'^n\pi(n-3)}+O(a), \qquad (44)\end{aligned}$$

where $\rho'=\rho/\rho_0$, ${}_2F_1(a,b;c,x)$ is the ordinary hypergeometric function, and

$$F_1(\rho') = {}_2F_1\left(\frac{n-2}{2},\frac{n-1}{2};\frac{n}{2};-\frac{(n-5)^2}{4\rho'^2}\right), \qquad (45)$$

$$F_2(\rho') = {}_2F_1\left(\frac{n-1}{2},\frac{n-1}{2};\frac{n+1}{2};-\frac{(n-5)^2}{4\rho'^2}\right), \qquad (46)$$

$$F_3(\rho') = {}_2F_1\left(\frac{n-1}{2},\frac{n}{2};\frac{n+2}{2};-\frac{(n-5)^2}{4\rho'^2}\right), \qquad (47)$$

$$F_4(\rho') = {}_2F_1\left(\frac{n-3}{2},\frac{n-3}{2};\frac{n-1}{2};-\frac{(n-5)^2}{4\rho'^2}\right). \qquad (48)$$

Clearly the above forms are not $O(a)$ to leading order; thus, the power law blobs do not formally capture the flow. Furthermore, since the conditions are also not satisfied when $\rho'=1$, the power-law blobs are incapable of capturing the no-slip boundary conditions. However, when these functions are plotted against ρ' for different n (Figure 2), we find that they are small for small n and increase as n increases. This suggests that although these representations cannot replicate the boundary conditions directly, when $n=6$ or $n=7$, the error induced by these terms may be small. This may explain why $n=7$ blobs have seemingly been successfully used in many problems, although in practice further validation is needed to be certain that they actually represent real flow.

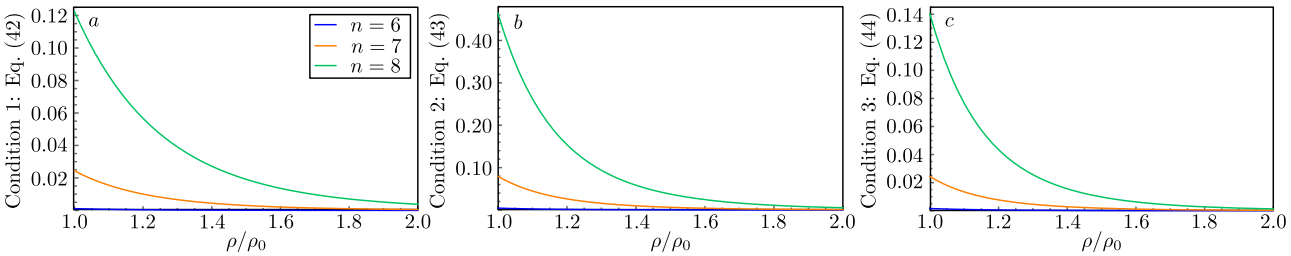

Figure 2. The value of near flow conditions for power-law blobs of $n = 6$ (blue), $n = 7$ (orange) and $n = 8$ (green). (**a**) Displays the result from condition Equation (37) (Equation (42)), (**b**) displays the result from condition Equation (38) (Equation (43)) and (**c**) displays the result from condition Equation (39) (Equation (44)).

Finally, we note that the same conclusion can be drawn by completing the inner region expansion of the resultant regularized Stokeslet. For example, when $n = 7$ the regularized Stokeslet from this blob has the form of Equation (8). If we expand this in the inner limit, we find the following:

$$\boldsymbol{S}^{\epsilon(i)}(\boldsymbol{x} - \boldsymbol{x_0}(t)) = \frac{\boldsymbol{I}(\delta^2 + 2h^2) + \rho^2 \boldsymbol{e_r e_r} - \rho\xi(\boldsymbol{e_r e_t} + \boldsymbol{e_t e_r}) + \xi^2 \boldsymbol{e_t e_t}}{8\pi a\sqrt{\delta^2 + h^2}^3} + O(a), \tag{49}$$

which can then be integrated to give:

$$8\pi \int_0^1 \boldsymbol{S}^{\epsilon(i)}(\boldsymbol{x} - \boldsymbol{x_0}(t))\, dt = \boldsymbol{I}\left(L_2 + \frac{2\rho^2 + 4h^2(s)}{\rho^2 + h^2(s)}\right) + \frac{2\rho^2}{\rho^2 + h^2(s)} \boldsymbol{e_r e_r} + L_2 \boldsymbol{e_t e_t}, \tag{50}$$

where $L_2 = \ln[4s(1-s)/(a^2(\rho^2 + h^2))]$. The inner structure clearly has a non-zero $\boldsymbol{e_r e_r}$ term that cannot be eliminated by any choice of h. Hence, this blob cannot remove this angular dependence and cannot satisfy the boundary conditions on the surface of the slender body when $\rho = \rho_0$. Therefore, it cannot be assumed a priori that the flow from a line of these regularized Stokeslets approximates the flow around a slender body. The presence of this $\boldsymbol{e_r e_r}$ term is directly related to Equation (43) containing an O(1) contribution. This is because the condition used in Equation (43) comes from the E_2 terms, which contain the difference in the leading order terms from a line of regularised Stokeslets and SBT in the $\boldsymbol{e_r e_r}$ direction.

5.2. Compact Blobs

Another class of blobs that can be used for regularized singularities are compact blobs. These blobs are zero beyond a certain radius and can significantly simplify the integration. Although such compact blobs regularize the singularity, they often generate discontinuities in the flow; thus, they are not used as often. For example, consider the following blob:

$$f_c(v) = \begin{cases} \frac{15}{32\pi}(21v^2 - 11) & v < 1 \\ 0 & v \geq 1 \end{cases}. \tag{51}$$

This blob isolates the regularization to within the slender body and is chosen such that the total dipole strength is the same as in classical slender-body theory. Given these conditions we expect that the flow outside the body should solve the unforced Stokes equations and identically match the slender-body flow. This can be verified directly with the far field condition, Equation (23), which sets the regularization parameter as

$$h = \rho_0, \tag{52}$$

and the near field conditions become

$$\int_{-s/(a\rho)}^{(1-s)/(a\rho)} (\zeta^2+1)\left[\int_1^\infty \left(\varrho-\varrho^2\right) f_c\left(\frac{\varrho\rho\sqrt{1+\zeta^2}}{h}\right) d\varrho\right] d\zeta = 0, \tag{53}$$

$$\int_{-s/(a\rho)}^{(1-s)/(a\rho)} \left[\int_1^\infty (\varrho^4-\varrho^2) f_c\left(\frac{\varrho\rho\sqrt{1+\zeta^2}}{h}\right) d\varrho\right] d\zeta = 0, \tag{54}$$

$$\int_{-s/(a\rho)}^{(1-s)/(a\rho)} \zeta^2\left[\int_1^\infty (\varrho^4-\varrho^2) f_c\left(\frac{\varrho\rho\sqrt{1+\zeta^2}}{h}\right) d\varrho\right] d\zeta = 0, \tag{55}$$

because $r\rho'\sqrt{1+\zeta^2} \geq 1$; thus, $f_c\left(r\rho'\sqrt{1+\zeta^2}\right) = 0$. Again, we observe that the regularization parameter ϵ equals half the body thickness, similar to those used in simulations; however, this representation also replicates all the near field conditions identically. Hence, a line of these compactly supported blobs could be used to asymptotically determine the flow around a slender body.

5.3. Gaussian Blobs

Finally we consider Gaussian blobs. These blobs decay to zero rapidly but are continuous and so can be thought of similar to an intermediate between the power law and the compact blobs. Gaussian blobs have the following form:

$$f_g(v) = \frac{1}{\pi^{3/2}} e^{-v^2}. \tag{56}$$

The far field condition for these blobs becomes

$$h = \rho_0, \tag{57}$$

similarly to the compact blob and power-law blob with $n = 7$ solution. However, in this case the near surface conditions become

$$\int_{-s/(a\rho)}^{(1-s)/(a\rho)} (\zeta^2+1)\left[\int_1^\infty \left(\varrho-\varrho^2\right) f_g\left(\frac{\varrho\rho\sqrt{1+\zeta^2}}{h}\right) d\varrho\right] d\zeta = -\frac{1}{4\pi\rho'^3}\int_{\rho'^2}^\infty \frac{e^{-u}}{u}\, du + O(a), \tag{58}$$

$$\int_{-s/(a\rho)}^{(1-s)/(a\rho)} \left[\int_1^\infty (\varrho^4-\varrho^2) f_g\left(\frac{\varrho\rho\sqrt{1+\zeta^2}}{h}\right) d\varrho\right] d\zeta = \frac{e^{-\rho'^2}}{2\pi\rho'^5} + O(a), \tag{59}$$

$$\int_{-s/(a\rho)}^{(1-s)/(a\rho)} \zeta^2\left[\int_1^\infty (\varrho^4-\varrho^2) f_g\left(\frac{\varrho\rho\sqrt{1+\zeta^2}}{h}\right) d\varrho\right] d\zeta = \frac{1}{4\pi\rho'^5}\left(e^{-\rho'^2} - \rho'^2\int_{\rho'^2}^\infty \frac{e^{-u}}{u}\, du\right) + O(a). \tag{60}$$

Again, the above evaluation shows that the exponential blobs do not satisfy the conditions; however, this error is exponentially small in ρ'^2 with the largest term being $1/2\pi$ when $\rho' = 1$. This again suggests that the asymptotic error from this regularization could be small; thus, it may still work for simulating the flow around the slender body. However, it would be important to validate the simulation sufficiently beforehand. We note that the difference between the SBT model and the line of Gaussian regularized Stokeslets at the surface can be constructed from the above conditions by using them to reconstruct the E_i when $\rho' = 1$.

6. Conclusions

In this paper, we compared the asymptotic flow from a line of regularized Stokeslets to that from a slender body. This was possible by comparing SBT with a matched asymptotic expansion of the flow from a generalised line of regularized Stokeslets. We focused on the flow far from the body and near the body surface as the SBT asymptotic representations

are expected to be the most valid in these regions. We found that any line of regularized Stokeslets can approximate the flow far from the body provided that the regularization parameter, ϵ, is equal to the thickness of the body, $a\rho_0$, multiplied by a constant that depends on the regularization blob, $(8\pi \int_0^\infty u^4 f(u)\, du/3)^{-1/2}$, Equation (23). This constant can be used for the unknown proportionality constant used in numerical simulations. The asymptotic flow near the surface of a slender body, however, could only be captured by specific regularisation blobs.

The regularized Stokeslets which are capable of asymptotically describing the flow near the surface of a slender body are found to satisfy three conditions (Equations (37)–(39)). These conditions depend on the tails of the regularization blob and are required to apply over a region. Importantly, these conditions must be met at the surface of the slender body if the drag from the line of regularized Stokeslets is to correctly predict the same force and torque on the body from a given motion. If it does not, then the representation cannot be assumed to describe the flow around a slender body. This restricts the types of regularization blobs that could be used when simulating a slender body with a line of regularised Stokeslets.

Finally, we tested these conditions on three blob types: power-law blobs, compact blobs and Gaussian blobs. While all could satisfy the far field condition without issue, we found that power-law blobs and Gaussian blobs could not satisfy the near field conditions anywhere. As such, these blobs cannot match the correct no-slip condition on the bodies surface and so models using these regularization's may not describe the desired system. Plots of the error suggested that these differences are small; thus, they may not make a large difference practically. The compact blobs investigated were found to satisfy all the conditions without issue. This means that, out of the three blobs considered, the compact blob is the best suited for modelling the behaviour of slender bodies with a line of regularised Stokeslets.

In this article, we restricted ourselves to spherically symmetric regularizations and focused on slender bodies with circular cross sections. It would be of interest to extend the results to non-spherically symmetric regularizations and slender bodies with non-circular cross sections to observe how the conditions change. Furthermore, slender-body theory has also been used in potential flow and diffusion problems; thus, the method could be extended to investigate the accuracy of a line of singularities for a slender body in those systems. Finally, we note that the only regularization we found that satisfied all the conditions was a compact blob; thus, it would be of interest to investigate any non-compact examples that can work.

Author Contributions: Conceptualization, L.K.; methodology, L.K.; formal analysis, B.Z.; investigation, B.Z.; writing—original draft preparation, B.Z.; writing—review and editing, L.K.; supervision, L.K.; project administration, L.K.; funding acquisition, L.K. Both authors have read and agreed to the published version of the manuscript.

Funding: L.K. was funded by Australian Research Council (ARC) under the Discovery Early Career Research Award scheme (grant agreement DE200100168).

Acknowledgments: The authors also thank Eric Lauga for useful discussions and advice.

Conflicts of Interest: The authors declare no conflict of interest.

References

1. Cox, R.G. The motion of long slender bodies in a viscous fluid Part 1. General theory. *J. Fluid Mech.* **1970**, *44*, 791. [CrossRef]
2. Lighthill, J. Flagellar Hydrodynamics: The John von Neumann Lecture, 1975. *SIAM Rev.* **1976**, *18*, 161–230. [CrossRef]
3. Batchelor, G.K. Slender-body theory for particles of arbitrary cross-section in Stokes flow. *J. Fluid Mech.* **1970**, *44*, 419–440. [CrossRef]
4. Keller, J.B.; Rubinow, S.I. Slender-body theory for slow viscous flow. *J. Fluid Mech.* **1976**, *75*, 705–714. [CrossRef]
5. Johnson, R.E. An improved slender-body theory for Stokes flow. *J. Fluid Mech.* **1979**, *99*, 411–431. [CrossRef]
6. Götz, T. Interactions of Fibers and Flow: Asymptotics, Theory and Numerics. Ph.D. Thesis, University of Kaiserslautern, Kaiserslautern, Germany, 2000.

7. Koens, L.; Lauga, E. The boundary integral formulation of Stokes flows includes slender-body theory. *J. Fluid Mech.* **2018**, *850*, R1. [CrossRef]
8. Andersson, H.I.; Celledoni, E.; Ohm, L.; Owren, B.; Tapley, B.K. An integral model based on slender body theory, with applications to curved rigid fibers. *Phys. Fluids* **2021**, *33*, 041904. [CrossRef]
9. Barta, E.; Liron, N. Slender Body Interactions for Low Reynolds Numbers—Part I: Body-Wall Interactions. *SIAM J. Appl. Math.* **1988**, *48*, 992–1008. [CrossRef]
10. Koens, L.; Montenegro-Johnson, T.D. Local drag of a slender rod parallel to a plane wall in a viscous fluid. *Phys. Rev. Fluids* **2021**, *6*, 064101. [CrossRef]
11. Kim, M.J.; Kim, M.J.; Bird, J.C.; Park, J.; Powers, T.R.; Breuer, K.S. Particle image velocimetry experiments on a macro-scale model for bacterial flagellar bundling. *Exp. Fluids* **2004**, *37*, 782–788. [CrossRef]
12. Das, D.; Lauga, E. Computing the motor torque of Escherichia coli. *Soft Matter* **2018**, *14*, 5955–5967. [CrossRef] [PubMed]
13. Higdon, J.J.L. A hydrodynamic analysis of flagellar propulsion. *J. Fluid Mech.* **1979**, *90*, 685. [CrossRef]
14. Barta, E.; Weihs, D. Creeping flow around a finite row of slender bodies in close proximity. *J. Fluid Mech.* **2006**, *551*, 1–17. [CrossRef]
15. Cummins, C.; Seale, M.; Macente, A.; Certini, D.; Mastropaolo, E.; Viola, I.M.; Nakayama, N. A separated vortex ring underlies the flight of the dandelion. *Nature* **2018**, *562*, 414–418. [CrossRef] [PubMed]
16. Rodenborn, B.; Chen, C.H.; Swinney, H.L.; Liu, B.; Zhang, H.P. Propulsion of microorganisms by a helical flagellum. *Proc. Natl. Acad. Sci. USA* **2013**, *110*, E338–E347. [CrossRef] [PubMed]
17. Gray, J.; Hancock, G.J. The Propulsion of Sea-Urchin Spermatozoa. *J. Exp. Biol.* **1955**, *32*, 802–814. [CrossRef]
18. Chattopadhyay, S.; Moldovan, R.; Yeung, C.; Wu, X. Swimming efficiency of bacterium *Escherichia coli*. *Proc. Natl. Acad. Sci. USA* **2006**, *103*, 13712–13717. [CrossRef]
19. Koens, L.; Zhang, H.; Moeller, M.; Mourran, A.; Lauga, E. The swimming of a deforming helix. *Eur. Phys. J. E* **2018**, *41*, 119. [CrossRef]
20. Zhang, X.; Chan, F.K.; Parthasarathy, T.; Gazzola, M. Modeling and simulation of complex dynamic musculoskeletal architectures. *Nat. Commun.* **2019**, *10*, 4825. [CrossRef]
21. Becker, L.E.; Koehler, S.A.; Stone, H.A. On self-propulsion of micro-machines at low Reynolds number: Purcell's three-link swimmer. *J. Fluid Mech.* **2003**, *490*, 15–35. [CrossRef]
22. Tătulea-Codrean, M.; Lauga, E. Asymptotic theory of hydrodynamic interactions between slender filaments. *Phys. Rev. Fluids* **2021**, *6*, 074103. [CrossRef]
23. Waszkiewicz, R.; Szymczak, P.; Lisicki, M. Stability of sedimenting flexible loops. *J. Fluid Mech.* **2021**, *919*, A14. [CrossRef]
24. Man, Y.; Page, W.; Poole, R.J.; Lauga, E. Bundling of elastic filaments induced by hydrodynamic interactions. *Phys. Rev. Fluids* **2017**, *2*, 123101. [CrossRef]
25. Cortez, R. The Method of Regularized Stokeslets. *SIAM J. Sci. Comput.* **2001**, *23*, 1204–1225. [CrossRef]
26. Cortez, R.; Fauci, L.; Medovikov, A. The method of regularized Stokeslets in three dimensions: Analysis, validation, and application to helical swimming. *Phys. Fluids* **2005**, *17*, 031504. [CrossRef]
27. Zhao, B.; Lauga, E.; Koens, L. Method of regularized stokeslets: Flow analysis and improvement of convergence. *Phys. Rev. Fluids* **2019**, *4*, 084104. [CrossRef]
28. Smith, D.J. A boundary element regularized Stokeslet method applied to cilia- and flagella-driven flow. *Proc. R. Soc. A Math. Phys. Eng. Sci.* **2009**, *465*, 3605–3626. [CrossRef]
29. Gallagher, M.T.; Smith, D.J. The art of coarse Stokes: Richardson extrapolation improves the accuracy and efficiency of the method of regularized stokeslets. *R. Soc. Open Sci.* **2021**, *8*, 210108. [CrossRef] [PubMed]
30. Nguyen, H.N.; Cortez, R. Reduction of the Regularization Error of the Method of Regularized Stokeslets for a Rigid Object Immersed in a Three-Dimensional Stokes Flow. *Commun. Comput. Phys.* **2014**, *15*, 126–152. [CrossRef]
31. Walker, B.J.; Curtis, M.P.; Ishimoto, K.; Gaffney, E.A. A regularised slender-body theory of non-uniform filaments. *J. Fluid Mech.* **2020**, *899*, A3. [CrossRef]
32. Cortez, R.; Nicholas, M. Slender body theory for Stokes flows with regularized forces. *Commun. Appl. Math. Comput. Sci.* **2012**, *7*, 33–62. [CrossRef]
33. Cortez, R. Regularized Stokeslet segments. *J. Comput. Phys.* **2018**, *375*, 783–796. [CrossRef]
34. Buchmann, A.; Fauci, L.J.; Leiderman, K.; Strawbridge, E.; Zhao, L. Mixing and pumping by pairs of helices in a viscous fluid. *Phys. Rev. E* **2018**, *97*, 023101. [CrossRef] [PubMed]
35. Martindale, J.D.; Jabbarzadeh, M.; Fu, H.C. Choice of computational method for swimming and pumping with nonslender helical filaments at low Reynolds number. *Phys. Fluids* **2016**, *28*, 021901. [CrossRef]
36. Nguyen, H.; Cortez, R.; Fauci, L. Computing Flows Around Microorganisms: Slender-Body Theory and Beyond. *Am. Math. Mon.* **2014**, *121*, 810. [CrossRef]
37. Nguyen, H.; Koehl, M.A.R.; Oakes, C.; Bustamante, G.; Fauci, L. Effects of cell morphology and attachment to a surface on the hydrodynamic performance of unicellular choanoflagellates. *J. R. Soc. Interface* **2019**, *16*, 20180736. [CrossRef]
38. Bouzarth, E.L.; Hutson, K.R.; Miller, Z.L.; Saine, M.E. Using Regularized Singularities to Model Stokes Flow: A Study of Fluid Dynamics Induced by Metachronal Ciliary Waves. In *An Introduction to Undergraduate Research in Computational and Mathematical Biology. Foundations for Undergraduate Research in Mathematics*; Birkhäuser: Cham, Switzerland, 2020; pp. 443–469. [CrossRef]

39. Olson, S.D.; Suarez, S.S.; Fauci, L.J. Coupling biochemistry and hydrodynamics captures hyperactivated sperm motility in a simple flagellar model. *J. Theor. Biol.* **2011**, *283*, 203–216. [CrossRef] [PubMed]
40. Montenegro-Johnson, T.D.; Koens, L.; Lauga, E. Microscale flow dynamics of ribbons and sheets. *Soft Matter* **2017**, *13*, 546–553. [CrossRef]
41. Ohm, L. Remarks on Regularized Stokeslets in Slender Body Theory. *Fluids* **2021**, *6*, 283. [CrossRef]
42. Kim, S.; Karrila, S.J. *Microhydrodynamics: Principles and Selected Applications*; Courier Corporation: Boston, MA, USA, 2005; p. 507.
43. Lamb, H. *Hydrodynamics*, 6th ed.; Cambridge University Press: Cambridge, UK, 1932; p. 605.
44. Pozrikidis, C. *Boundary Integral and Singularity Methods for Linearized Viscous Flow*; Cambridge University Press: Cambridge, UK, 1992; p. 259.
45. Chwang, A.T.; Wu, T.Y. Hydromechanics of low-Reynolds-number flow. Part 2. Singularity method for Stokes flows. *J. Fluid Mech.* **1975**, *67*, 787–815. [CrossRef]
46. Montenegro-Johnson, T.; Smith, A.; Smith, D.; Loghin, D.; Blake, J. Modelling the fluid mechanics of cilia and flagella in reproduction and development. *Eur. Phys. J. E Soft Matter* **2012**, *35*, 111. [CrossRef]
47. Montenegro-Johnson, T.D. Microtransformers: Controlled microscale navigation with flexible robots. *Phys. Rev. Fluids* **2018**, *3*, 062201. [CrossRef]
48. Ainley, J.; Durkin, S.; Embid, R.; Boindala, P.; Cortez, R. The method of images for regularized Stokeslets. *J. Comput. Phys.* **2008**, *227*, 4600–4616. [CrossRef]
49. Cortez, R.; Varela, D. A general system of images for regularized Stokeslets and other elements near a plane wall. *J. Comput. Phys.* **2015**, *285*, 41–54. [CrossRef]
50. Hinch, E.J. *Perturbation Methods*; Cambridge University Press: Cambridge, UK, 1991; p. 160.
51. Lauga, E. Bacterial Hydrodynamics. *Annu. Rev. Fluid Mech.* **2016**, *48*, 105–130. [CrossRef]
52. Gaffney, E.A.; Gadêlha, H.; Smith, D.J.; Blake, J.R.; Kirkman-Brown, J.C. Mammalian Sperm Motility: Observation and Theory. *Annu. Rev. Fluid Mech.* **2011**, *43*, 501–528. [CrossRef]
53. Katsamba, P.; Michelin, S.; Montenegro-Johnson, T.D. Slender Phoretic Theory of chemically active filaments. *J. Fluid Mech.* **2020**, *898*, A24. [CrossRef]
54. Borker, N.S.; Koch, D.L. Slender body theory for particles with non-circular cross-sections with application to particle dynamics in shear flows. *J. Fluid Mech.* **2019**, *877*, 1098–1133. [CrossRef]
55. Koens, L.; Lauga, E. Slender-ribbon theory. *Phys. Fluids* **2016**, *28*, 013101. [CrossRef]
56. Mori, Y.; Ohm, L. Accuracy of slender body theory in approximating force exerted by thin fiber on viscous fluid. *Stud. Appl. Math.* **2021**, *147*, 127–179. [CrossRef]
57. Mori, Y.; Ohm, L.; Spirn, D. Theoretical Justification and Error Analysis for Slender Body Theory. *Commun. Pure Appl. Math.* **2020**, *73*, 1245–1314. [CrossRef]
58. Mori, Y.; Ohm, L.; Spirn, D. Theoretical Justification and Error Analysis for Slender Body Theory with Free Ends. *Arch. Ration. Mech. Anal.* **2020**, *235*, 1905–1978. [CrossRef]